Supporting Information

Controllable synthesis of silver cyanamide as a new semiconductor photocatalyst under visible-light irradiation

Wei Zhao,[a,b,‖] Yufeng Liu,[a,‖] Jiajia Liu,[b,‖] Ping Chen,[a] I-Wei Chen,[c] Fuqiang Huang,[a,b,]* and Jianhua Lin[b,]*

[a] CAS Key Laboratory of Materials for Energy Conversion and State Key Laboratory of High Performance Ceramics and Superfine Microstructure, Shanghai Institute of Ceramics, Chinese Academy of Sciences, Shanghai 200050, P.R. China

[b] Beijing National Laboratory for Molecular Sciences and State Key Laboratory of Rare Earth Materials Chemistry and Applications, College of Chemistry and Molecular Engineering, Peking University, Beijing 100871, China

[c] Department of Materials Science and Engineering, University of Pennsylvania, Philadelphia, PA 19104, USA

* Correspondence should be addressed to huangfq@mail.sic.ac.cn, jhlin@pku.edu.cn.

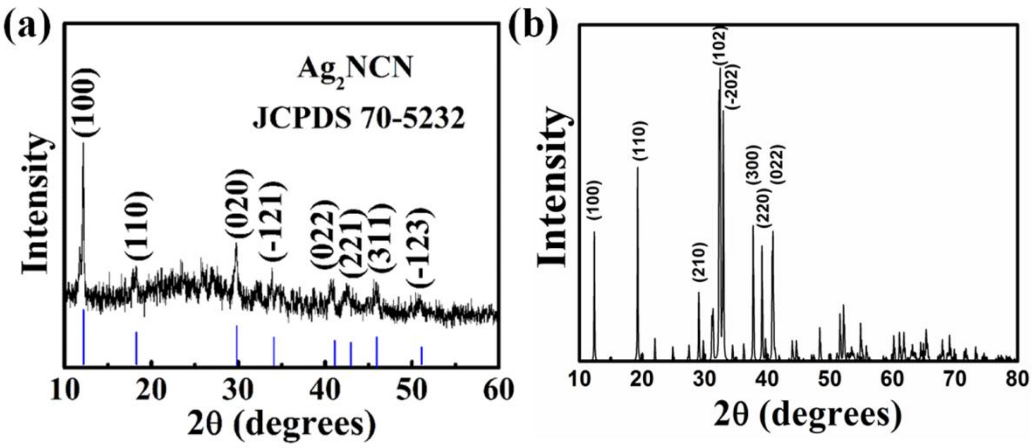

Figure S1. (a) XRD pattern of the as-prepared Ag_2NCN nanoparticles. Bottom: reference JCPDS peaks. (b) Calculated XRD pattern of Ag_2NCN, with the strongest peak at (102).

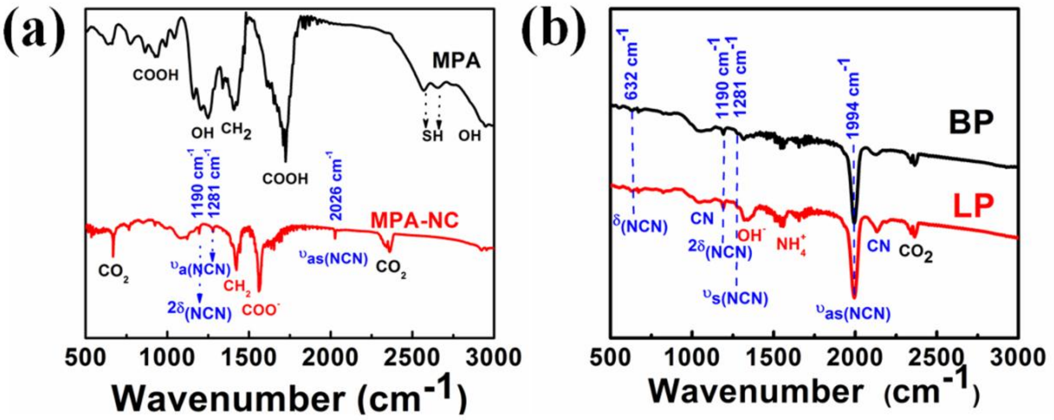

Figure S2. FTIR spectra of (a) MPA and MPA-capped Ag_2NCN NP and (b) Ag_2NCN microparticles (BP and LP sample).

In Figure S2a, we compare the FTIR spectra of MPA and MPA-capped NP. The NP sample was prepared in strong basic aqueous solution, so both -SH and -OH of MPA (formula: $SH\text{-}CH_2\text{-}CH_2\text{-}COOH$) were deprotonated. Therefore, -SH and -OH vibrations are absent in MPA-capped NP. The characteristic peaks of Ag_2NCN are marked in blue in Figure S2. The other peaks are also identified to be due to either MPA or environment (CO_2, etc.).

The FTIR spectra of microparticles (BP and LP) which have no MPA ligand are shown in Figure S3b. The strongest absorption peak located at 1994 cm^{-1} can be ascribed to the asymmetric stretching vibration of NCN group ($\upsilon_{as(NCN)}$). This value is consistent to the reported one (1995 cm^{-1}) in the reference ("Electronic and the stability of inorganic cyanamides," M. J. Sole, A. D. Yoffe. *Proc. R. Soc. Lond. A*, **1964**, *277*, 498.). The intensities for NCN symmetric stretching ($\upsilon_{s(NCN)}$: 1281 cm^{-1}) and NCN deformation vibration ($\delta_{(NCN)}$: 633 cm^{-1} and $2\delta_{(NCN)}$: 1190 cm^{-1}) are weaker, which was also found in the above reference.

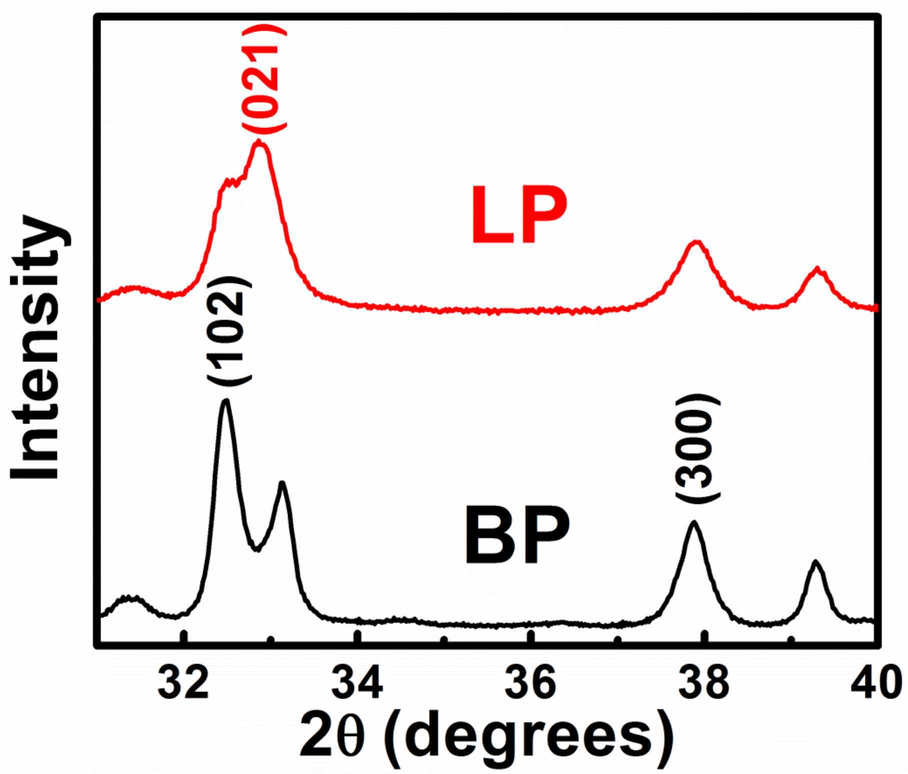

Figure S3. XRD patterns of the as-prepared Ag_2NCN microparticles at 2θ from 31° to 40°.

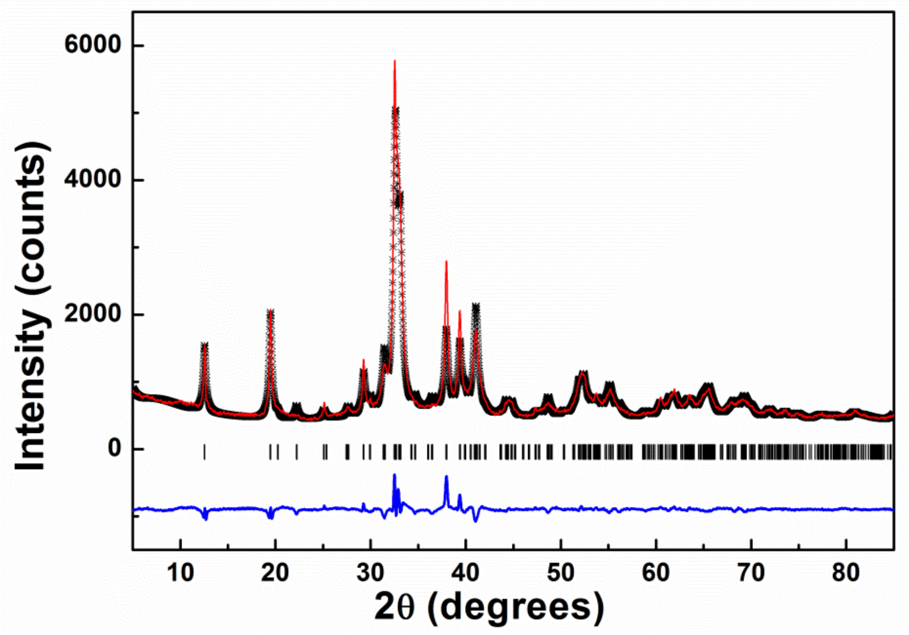

Figure S4. Observed (crosses) and calculated (red) XRD patterns along with their difference spectra (blue) from Rietveld refinement of Ag_2NCN sample (heavily ground BP). (R_p= 5.43%, R_{wp} = 7.86%.) Positions of Bragg reflections marked by short bars.

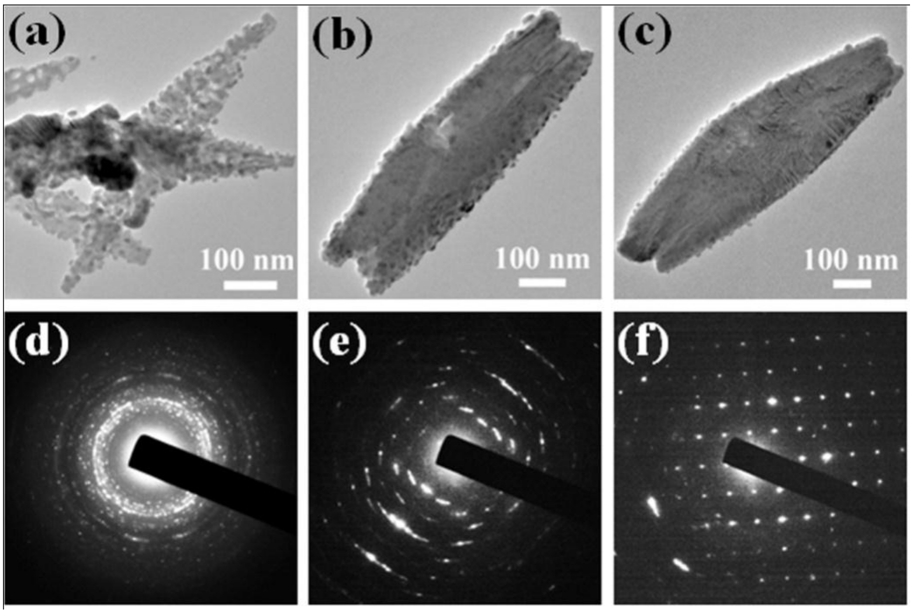

Figure S5. TEM images and SAED patterns of LP samples obtained at $[NH_3]/[Ag^+]$ = 37.5:1 with increasing reaction time: (a) and (d) 0.5 h, (b) and (e) 8 h, (c) and (f) 24 h.

Growth of microparticles. XRD Patterns of microparticles (LP and BP) shown in Figure S3 have different relative intensities for different peaks, and both are different from Figure S1 because of texturing. To investigate the growth mechanism, TEM characterization of LP microparticles harvested after various reaction times was conducted as shown in Figure S5. Clearly, each platelet obtained after reaction for 0.5 h consists of many nanoparticles. Figure S5b-5c reveal recrystallization of nanoparticles occurring over time improving the crystallinity of the platelets, which maintained about the same overall morphology. This is confirmed by the selected area electron diffraction (SAED) patterns (Figure S5d-f) of LP microparticles, which dramatically sharpened with reaction time, changing from fuzzy polycrystaline diffraction rings to sharp single-crystalline diffraction spots. This suggests that the growth mechanism of LP Ag_2NCN microparticles is oriented attachment and coarsening: (a) initially a loose aggregation of nanoparticles of relatively random crystallographic orientations forms, (b) this is followed by a self-organization of adjacent particles rotating into a common crystallographic orientation, presumably to realize lower interfacial energies between similarly oriented crystals, and (c) finally Oswald ripening occurs by removing low-angle grain boundaries between grains (nanocrystals), forming a Ag_2NCN single-crystal. We have also examined BP samples and found all of them to be single crystals (see Figure S6).

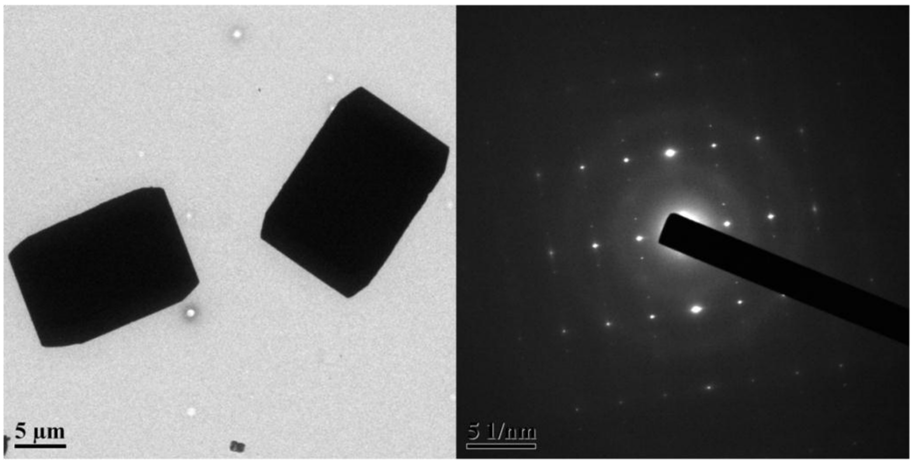

Figure S6. TEM image and SAED pattern of BP sample obtained at $[NH_3]/[Ag^+]$ = 600:1.

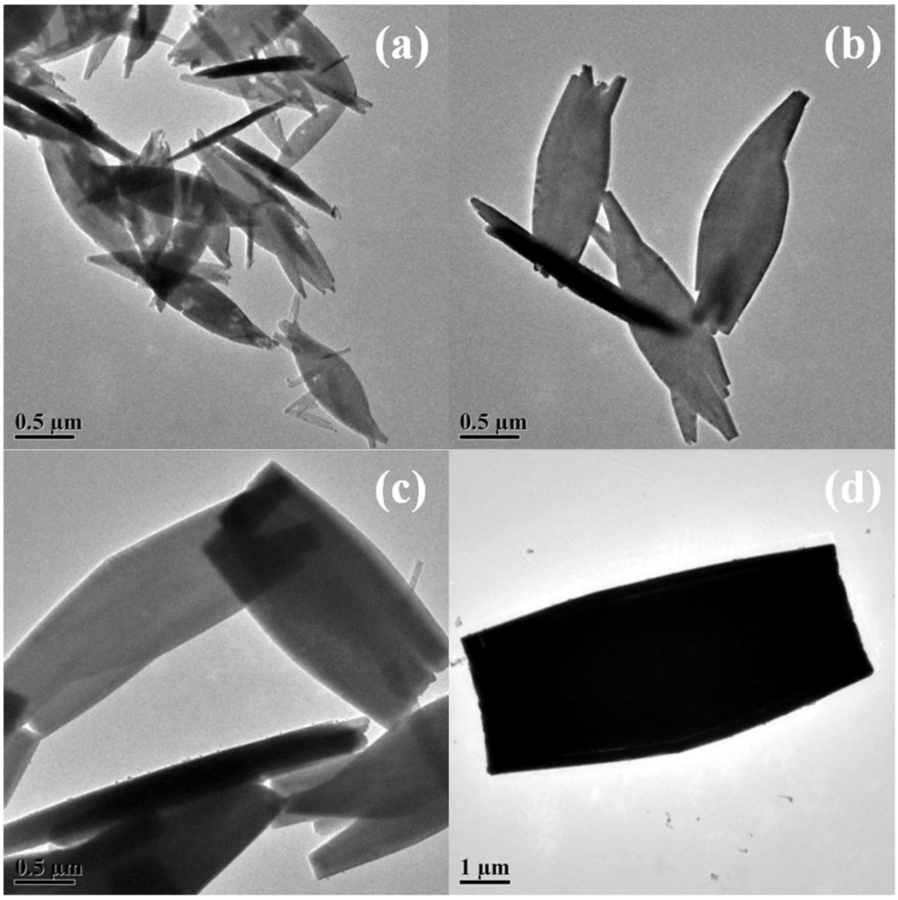

Figure S7. TEM images of Ag_2NCN microparticles prepared at $[NH_3]/[Ag^+]$ molar ratios of (a) 10:1, (b) 100:1, (c) 200:1, (d) 400:1.

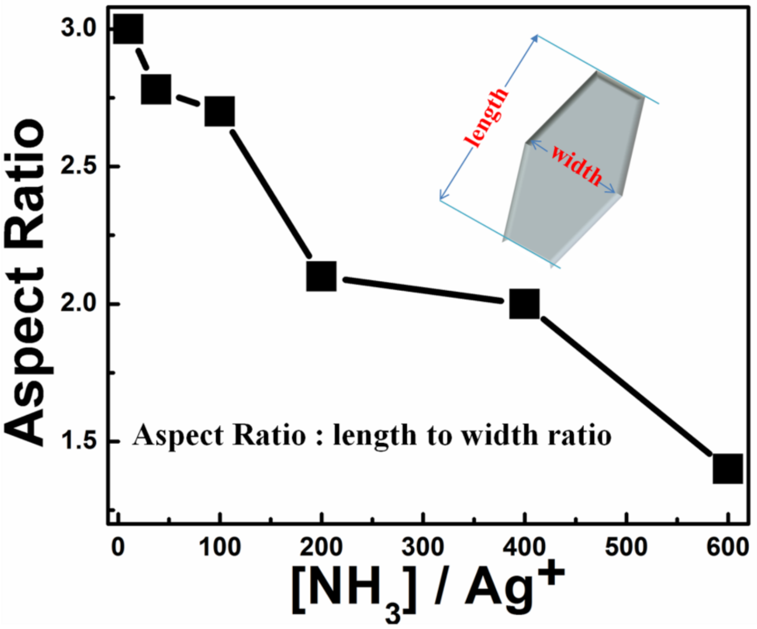

Figure S8. The relationship between aspect ratio of Ag_2NCN microparticles and $[NH_3]/[Ag^+]$ molar ratios.

Table S1 Elemental analysis of Ag_2NCN sample (BP).

Element	**Nominal Ratio (wt%)**	**Measured Ratio (wt%)**		**Average Ratio (wt%)**
		1st batch	2nd batch	
Ag [b]	84.35	82.54	82.70	82.63
C [a]	4.70	5.04	5.14	5.09
N [a]	10.95	11.18	11.03	11.11
O [c]	0	1.14	1.20	1.17

[a] Measured by a CHN analyzer. [b] Measured by X-ray fluorescence spectrometer. [c] Oxygen contamination may be attributed to the absorbed water or crystallization water.

Crystal structure of Ag_2NCN (Table S2-S3**)**. The crystal structure of Ag_2NCN can be considered to consist of infinite planar zigzag chains of Ag1-N1-C-N2-Ag1-N1-C-N2 (Chain 1). These chains are connected by Ag1, Ag2 and Ag3 via N1 to form a three dimensional structure. The Ag1 atom is tetrahedrally coordinated to four N atoms (two N in the same planar chain, two N in two other chains) with two short Ag1–N1 (2.204(15) Å) and Ag1–N2 (2.191(13) Å) and two long Ag1–N2 (2.577(13) Å, 2.736(14) Å), and the latter two long bonds also form N2-Ag1-N2-Ag1-N2 chains (Chain 2). Each Ag2 or Ag3 is linearly coordinated to two N1 atoms to form zigzag N1-Ag-N1-Ag-N1 chains (Chain 3). In each NCN unit, N1 is coordinated to Ag1, Ag2, and Ag3, and N2 is coordinated to three Ag1. Interestingly, many relatively short Ag-Ag distances (3.005(1)–3.341(2) Å) are observed.

Table S2. Position parameters of crystal structure for Ag_2NCN.

Atom	***x***	***y***	***z***
Ag1	0.6677(3)	0.1959(2)	0.1726(3)
Ag2	0	0	0
Ag3	0	0	0.5
C	0.292(2)	0.178(3)	0.313(2)
N1	0.181(2)	0.015(2)	0.293(2)
N2	0.608(2)	0.839(2)	0.177(2)

* *a=7.308(3) Å, b=6.011(2) Å, c=6.686(3) Å,* β *=102.124(9)°; P21/c (No.14); Z=4.*

Table S3. Selected bond lengths (Å) for Ag_2NCN.

C–N1	1.27(2)	Ag2–N1	2.122(15) ×2
C–N2	1.204(19)	Ag3–N1	2.105(14) ×2
Ag1–N	1.204(15)	Ag1–Ag2	3.129(2)
Ag1–N2	2.191(13)	Ag1–Ag3	3.137(2)
Ag1–N2	2.577(13)	Ag2–Ag3	3.005(1)
Ag1–N2	2.736(14)	Ag2–Ag3	3.341(2)

Partial density of states of Ag and N

The oxidation states of Ag, C, and N in Ag_2NCN are +1, +4, and −3, respectively. The analysis of partial density of states (PDOS) on Ag and N was performed, as shown in Figure S7 and Figure S8. The Ag1 atoms have more 4*d* states at VBM than Ag2 and Ag3, but the opposite holds at CBM. The PDOS of N1 and N2 at VBM are almost the same, but PDOS of N1 is larger than that of N2 at CBM. Therefore, the zigzag chain of N1-Ag-N1-Ag-N1 (Chain 3, containing Ag2 and Ag3) is more electrophilic (*n*-type) than N2-Ag1-N2-Ag1-N2 (Chain 2). The results support the scheme in Figure 5.

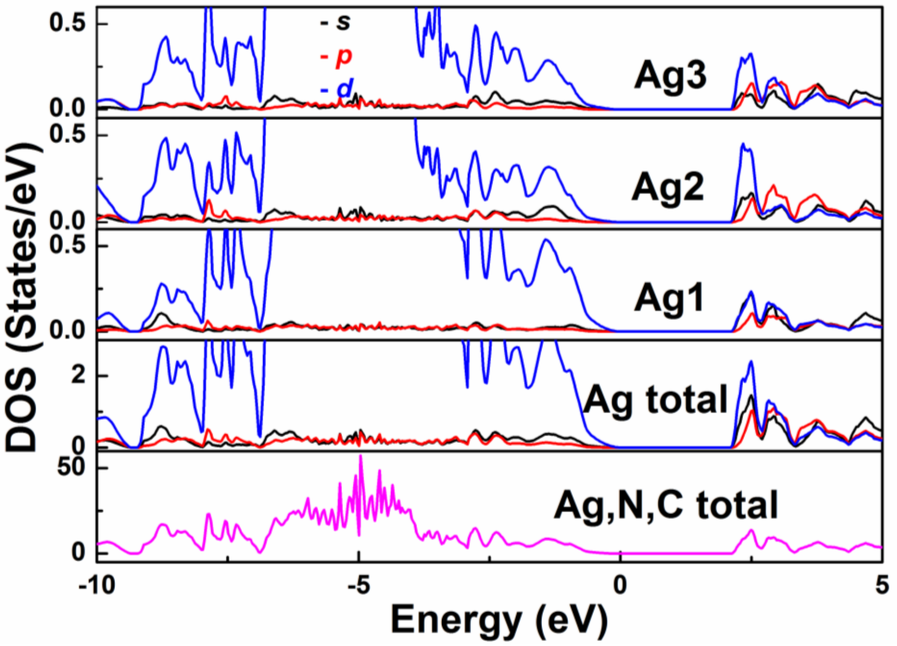

Figure S9. Partial DOS of Ag (Ag1, Ag2, Ag3).

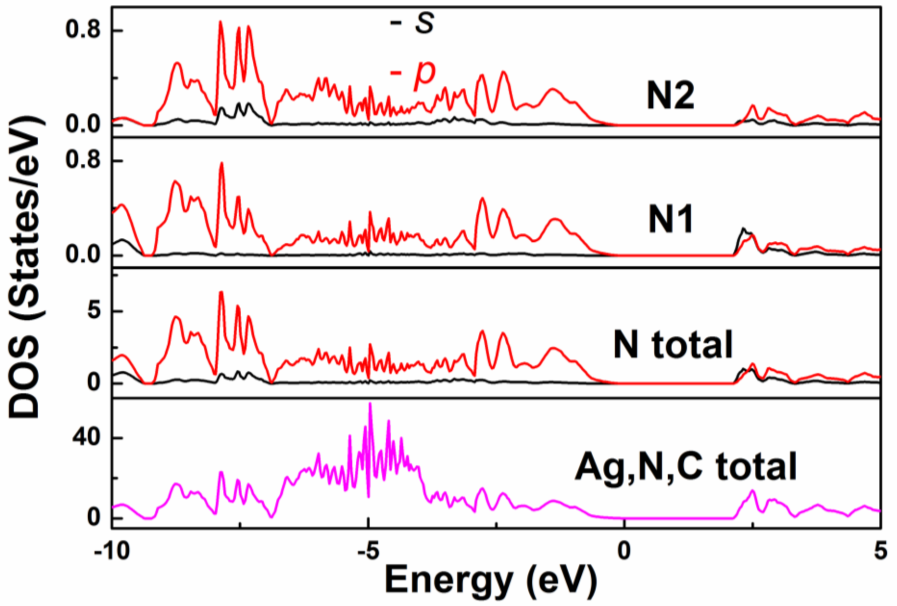

Figure S10. Partial DOS of N (N1, N2).

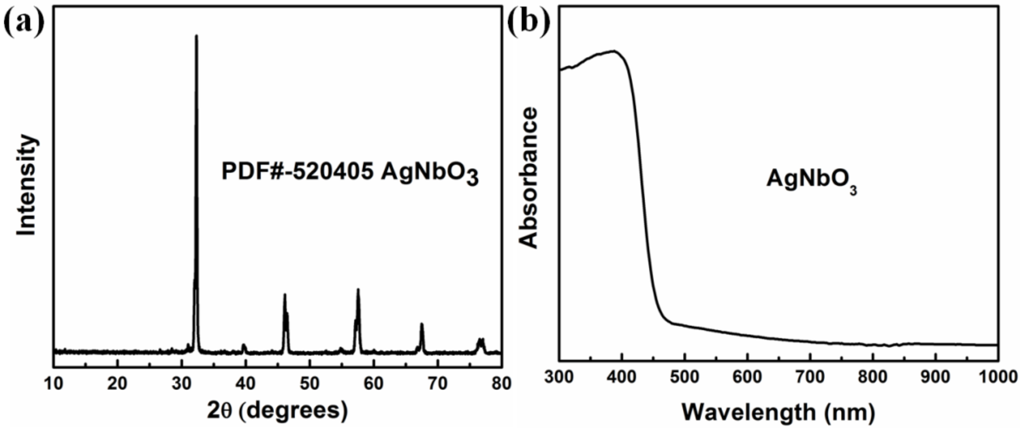

Figure S11. The XRD pattern and absorption property of as-prepared $AgNbO_3$ powder. All diffraction peaks can be indexed to orthorhombic structure of $AgNbO_3$ (JCPDS PDF# 52-0405).